Zircon U-Pb ages of Permian-Triassic granitoids in the southeastern Laoelin-Grodekov belt, Primorye, Far East Russia: correlation with the Hida belt in central Japan via the Yamato Ridge in the Sea of Japan

Yukio Isozaki[1]*, Ryo Hasegawa[1], Tomohito Nakano[1], Yukiyasu Tsutsumi[2], Victor Nechaev[3], Yuri Zakharov[3] and Alexander Popov[3]

[1]Department of Earth Science and Astronomy, The University of Tokyo, Komaba, Meguro, Tokyo153–8902, Japan
[2]Department of Geology and Paleontology, National Museum of Nature and Science, Amakubo, Tsukuba 028–0005, Japan
[3]Far East Geological Institute, Far Eastern Branch, Russian Academy of Sciences, Vladivostok 690022, Russia
*Author for correspondence: isozaki@ea.c.u-tokyo.ac.jp

Abstract For geological characterization of the boundary zone between the Khanka and North China continental blocks in Far East Asia, U-Pb ages of zircons were measured by laser-ablation inductively coupled plasma-mass spectrometry (LA-ICPMS) for undated five arc-type granitoids in southwestern Primorye, Russia. From granitoids in the Andreevka area in the eastern Laoelin-Grodekov (LG) belt along the Sea of Japan, we newly obtain four U-Pb ages of the Early-Middle Triassic and one age of the late Permian. Together with previous geochronological and geochemical data from Primorye and west-neighboring Jilin (China) and Hamgyon-Buk (North Korea), the newly obtained ages confirm the regional occurrence of Wuchiapingian (late Permian) to Anisian (middle Triassic) granitoids in the LG belt between the Khanka and North China blocks, which probably formed a large-scale arc batholith. These granitoid ages, together with the co-occurrence with the Jurassic granitoids suggest the geological correlation between the LG belt in the mainland Primorye and the Hida belt in central Japan, via the Yamato ridge in the middle of the Sea of Japan. The LG belt, Yamato ridge, and Hida belt altogether mark the eastern (or Pacific-side) limit for the co-occurrence of Permo-Triassic and Jurassic arc-type granitoids in Far East Asia.

Key words: Permian-Triassic, granitoid, zircon U-Pb age, Laoelin-Grodekov belt, Hida belt

Introduction

One of the prominent island arc systems in East Asia is represented by the modern Japanese Islands, which tectonically became separated from the mainland Asia by the Miocene back-arc spreading (e.g., Otofuji *et al.*, 1986; Tamaki, 1993). For reconstructing the paleogeography of pre-Miocene East Asia, profound understanding of geology of the circum-Sea of Japan region is inevitable; in particular, the pre-Cenozoic geological comparison is critical between Primorye of Far East Russia and Japan over the greatest distance (ca. 1,000 km) across the Sea of Japan. To date, various common units were identified in Primorye and Japan; e.g. Paleozoic-

Mesozoic granitoids, high-P/T metamorphic rocks, ophiolites, cover sedimentary rocks, and Mesozoic accretionary complexes, although most of them were fragmented into smaller pieces particularly in Japan (Kojima, 1989; Kemkin *et al.*, 1997; Kojima *et al.*, 2000; Ishiwatari and Tsujimori, 2003; Tsutsumi *et al.*, 2014; Khanchuk *et al.*, 2016; Isozaki *et al.*, 2017). In addition, common aspects of the Paleozoic-Mesozoic fossil fauna/flora were also recognized in Primorye and Japan (e.g. Tazawa, 1991, 2018; Zakharov *et al.*, 1992; Ehiro, 2001; Isozaki, 2019). These suggest their primary connection prior to the opening of the Sea of Japan; nonetheless, various hypotheses on tectonic model and paleogeographical reconstruction ever proposed (e.g. Hiroi, 1981; Tamaki, 1988; Zonenshain *et al.*, 1990; Clu-

zel *et al.*, 1991; Ishiwatari and Tsujimori, 2003; Izosov and Konovalov, 2005; Oh, 2006; Zhao *et al.*, 2013; Khanchuk *et al.*, 2016; Isozaki, 2019) have never reached consensus.

The overall structure of the Phanerozoic orogen in Japan indicates that all the above-listed orogenic units in Primorye and Japan have essentially formed through the long-term subduction processes from the paleo-Pacific (Panthalassan) side; namely they once belonged to a single but over 2,000 km-long arc-trench system. This subduction-induced active continental margin developed since the Cambrian along a major continental block, of which name was lately given as the Greater South China (Isozaki *et al.*, 2014, 2015, 2017).

As originally pointed out by Takahashi (1983), the distribution pattern of Paleo-Mesozoic granit-oids in East Asia provides the most reliable clue for the pre-Miocene paleogeographic reconstruction because granitoids represent the majority of newly forming crustal material in subduction-related oro-gens. As well as in Japan, various granitoids of the Khanka block in southern Primorye and north-neighboring Heilongjian in China have been recently dated by zircon U-Pb dating methods, in addition to the K-Ar and Rb-Sr dating systems, and their ages are confirmed to range mostly in the early Paleozoic, and also in the Cretaceous (e.g. Khan-chuk *et al.*, 2010; Cao *et al.*, 2011; Yang *et al.*, 2015; Nevolin *et al.*, 2015; Tsutsumi *et al.*, 2014, 2016). More Paleozoic and Mesozoic granitoids are exposed extensively in the Laoelin-Gorodekov (LG) belt on the west of the Khanka block, near the bor-der among Russia, China, and North Korea along the northern coast of the Sea of Japan (Fig. 1A). These granitoids were recently dated by zircon U-Pb method, in particular, in Jilin, China, and also in Hamgyong-Buk, North Korea (Ma *et al.*, 2013; Chen *et al.*, 2017; Zhai *et al.*, 2016), nonetheless, not much from Primorye, except for two reports on late Permian ages (Khanchuk *et al.*, 2010; Kruk *et al.*, 2015).

For providing more strict constraints to the paleo-geographical correlation/reconstruction between Primorye and Japan, we analyzed five granitoids samples from the Andreevka area of the L-G belt in southwestern Primorye (Fig. 1), particularly for zir-con U-Pb dating by laser-ablation inductively cou-
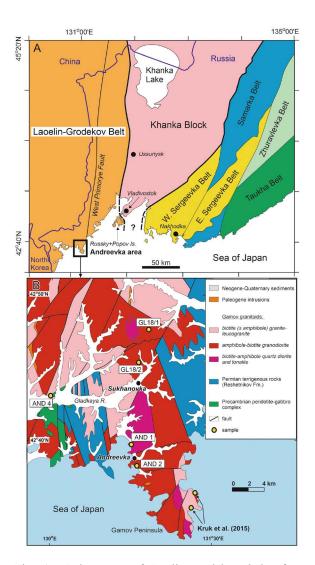

Fig. 1. Index map of Laolin-Grodekov belt after Malinovsky and Golozubov (2021) (A), and geo-logic sketch map (B) of Andreevka area in Laoe-lin-Grodekov belt in southwestern Primorye, Far East Russia, after State Geological map of the Rus-sian Federation on a Scale 1 : 200,000 Khanka Series. sheets K-52-XII and K-52-XVIII (2004) and Kruk *et al.* (2015) with five sample localities of granitoids for dating in this study.

pled plasma-mass spectrometry (LA-ICPMS). On the basis of newly obtained zircon U-Pb ages from the granitoids, i.e., one late Permian and four early-middle Triassic, this article discusses their geologi-cal significance for the LG belt in Primorye, and proposes an alternative correlation scheme with SW Japan, in particular, with the Hida belt in central Japan via the Yamato ridge in the midst of the Sea of Japan.

Geologic Setting

The geotectonic framework of southern Primorye

is characterized largely by the N-S trending zonal arrangement of multiple orogenic units (e.g. Mel'nikov and Izosov, 1984; Zakharov *et al.*, 1992; Khanchuk *et al.*, 1996; Fig. 1A). The Khanka block forms a prominent continental unit, ca. 500 km long in NE-SW and ca. 200 km wide in N-S directions, which extends northward into the southern Heilongjiang, China, across the Khanka Lake on the border. This block is composed of a wide variety of deformed/metamorphosed Paleozoic rocks, including gneiss-schists, granitoids, and sedimentary rocks, with unexposed Proterozoic basement with crustal/mantle signatures (Zhang *et al.*, 2010; Wang *et al.*, 2015; Maksimov and Sakhno, 2018), and also with covering Paleozoic-Mesozoic strata of marine/non-marine facies. The north-neighboring Jiamusi and Bureya blocks both in China and Primorye (Fig. 1A) share similar geologic components with the Khanka block, as recently confirmed by detrital zircon analyses, and they represent the northern extensions of the latter (Zhou *et al.*, 2010; Yang *et al.*, 2018; Ovchinnikov *et al.*, 2019).

On the eastern side of the Khanka block, plural belts of subduction-related origin occur; i.e., Sergeevka, Samarka, Zuravlevka, and Taukha belts (e.g. Kojima et al,. 2000; Kemkin, 2012; Khanchuk *et al.*, 1996, 2016; Fig. 1A), which are composed of accretionary complexes, blueschists, ophiolites, arc igneous complexes, and covering sedimentary sequences. As these elements are reasonably correlated with the coeval counterparts in NE and SW Japan (Kojima *et al.*, 2000; Ishiwatari and Tsujimori, 2003; Isozaki *et al.*, 2017), all these units totally belong to the Phanerozoic subduction-related orogenic belt along the Pacific-rim, i.e., *Nipponides* (Sengör and Natal'in, 1996), that developed along the Pacific side of the Greater South China (GSC) continental block (Isozaki *et al.*, 2014, 2017; Isozaki, 2019) prior to the Miocene opening of the Sea of Japan (e.g. Otofuji *et al.*, 1981; Tamaki, 1993).

The western side of the Khanka block has been traditionally defined by the N-S running West Primorye fault that separates the Khanka block from the Laoelin-Grodekov (LG) belt to the west (Khanchuk *et al.*, 1996; Fig. 1A), which was previously called "Tuman Basin" (Lee, 1987) or "Tumanggan Fold Belt" (Paek *et al.*, 1993) in Korea. Some recent studies, however, shifted the position of the western

boundary of the Khanka block for ca. 30 km to the west from the original line (Golozubov and Khanchuk, 2021; Golozubov and Simanenko, 2021) without giving clear explanation. Nonetheless, the LG belt corresponds to a transitional zone between the Khanka (GSC) block and the North China block further on the west, in other words, to the southeasternmost end of the Paleozoic Solonker suture (Xiao *et al.*, 2003). The Solonker suture represents the southern margin of the Central Asian orogenic belt (CAOB) or of the Paleo-Asian Ocean in the past (Jahn, 2000; Parfenov *et al.*, 2003; Wilde, 2015).

The LG belt, ca. 200 km wide in E-W direction, comprises mid-Paleozoic to Triassic volcano-sedimentary units intruded by Permian and Mesozoic granitoids, which were covered unconformably by non-metamorphosed Mesozoic strata of marine and non-marine facies (e.g., Zakharov *et al.*, 1992; Paek *et al.*, 1993; Khanchuk *et al.*, 2006; Ma *et al.*, 2016; Nevolin *et al.*, 2012). In addition, some small fragments of "Precambrian" metamorphic and ophiolitic rocks occur sporadically, however, their ages were not sufficiently constrained as depicted in State Geologic Map of Russian Federation in 1/200,000 scale, 2004; SGM afterwards). Early Silurian strata (Kordonka Formation) possess signatures of a volcanic arc (Malinovsky and Golozubov, 2021). The "Permo-Triassic" strata, composed of terrigenous clastics with minor amounts of limestones, were metamorphosed by numerous intrusions; nonetheless, they barely yield Carboniferous-Permian fossils of the Tethyan-Boreal mixed fauna and also Angaran and Cathaysian mixed floras (e.g., Noda, 1958; Huang, 1991a, 1991b; Tazawa, 1991; Zakharov *et al.*, 1992; Paek *et al.*, 1993; Kotlyar, 2006; Du *et al.*, 2021). The Late Triassic Talminsky complex consists of andesites and dacites with subduction-related geochemical signatures (Chashchin *et al.*, 2020).

The Andreevka area in coastal southwestern Primorye exposes for ca. 50 km-wide southeastern margin of the LG belt, of which the eastern boundary has been regarded as the West Primorye fault running in N-S direction off the Gamov peninsula (Fig. 1A). According to SGM, this area is underlain mostly by the "Permian" terrigenous clastics (Reshetnikov Fomation), which suffered contact metamorphism, partly baked up into hornfels, by

the Permian and younger granitoids (Nevolin, 2012; Kruk *et al.*, 2015). All these rocks are structurally aligned in N-S direction.

Pre-Cenozoic granitoids around the Andreevka town (Fig. 1B), traditionally called the Gamov and Gvozdevo complexes (e.g. Izosov and Konovalov, 2005), occur in an area of ca. 60 km wide both in N-S and E-W directions. These granitoids are composed mainly of granite, granodiorite, tonalite, and quartz diorite with minor amount of diorite and gabbro, most of which have geochemical characteristics of calc-alkaline, partly with high-K, and of I-type nature (Kruk *et al.*, 2015; Kharchenko and Valitov, 2018). Two age groups were discriminated for these granitoids, i.e., Permian and Jurassic ones, based on biotite K-Ar ages (SGM). Lately, Kruk *et al.* (2015) first reported two U-Pb ages of zircons, i.e., 259 Ma (Wuchiapingian, late Permian) for a leucogranite and

254 Ma (Wuchiapingian) for a tonalite, from the southeastern margin of Gamov peninsula (Fig. 1B); nonetheless, as to these granitoids in the near-border area to the west, a ca. 30 km-wide domain remains blank in age data to be filled by the present study.

Samples

We collected five granitoids from the following localities in the Andreevka area near the Gamov peninsula, in southwestern Primorye (Fig. 1B). All these granitoids of the Gamov intrusion were not dated before. More detailed petrography and geochemistry of these rocks will be reported elsewhere.

AND1: a medium-grained quartz diorite exposed along a local road near a small pass on the north of the Andreevka township (42°40′N; 131°08′E). The rock at this locality was mapped as a Permian intru-
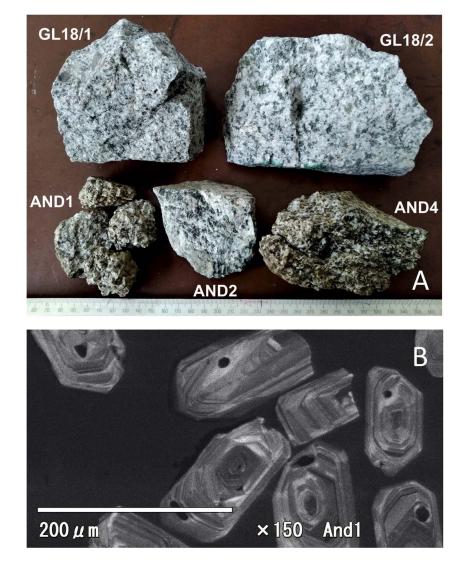

Fig. 2.　Photographs of five hand specimens of Gamov granitoids (A) and examples of cathodoluminescence images of dated zircons from AND1 with oscillatory zoning texture (B).

sion by SGM and Kruk *et al.* (2015).

AND2: a coarse-grained biotite-amphibole granodiorite (Fig. 2A) exposed along a coast-line local road on the south of the Andreevka township (42°39′N; 131°08′E). This granodiorite was mapped as a Permian intrusion (*ditto*).

AND4: a medium-grained biotite granite exposed along a highway on the west of the Sukhanovka village (42°43.378′N; 131°00.890′E). This granite, slightly weathered, was mapped as a Jurassic intrusion by SGM.

GL18/1: a medium-grained biotite-amphibole quartz granodiorite (Fig. 2B) exposed along a highway, ca. 8 km to the north of the Sukhanovka village (42°47.424′N; 131°09.873′E). This granodiorite was mapped as a Permian intrusion by SGM.

GL18/2: a coarse-grained amphibole-biotite granodiorite (Fig. 2B) exposed in a quarry near a highway, ca. 3 km to the north of the Sukhanovka village (42°45.088′N; 131°08.683′E). This granodiorite was mapped as a Permian intrusion by SGM.

Analytical Procedures

Zircon grains were handpicked from heavy fractions that were separated from the rock samples by standard crushing and heavy-liquid techniques at Department of Earth Science and Astronomy, The University of Tokyo. The separated zircon grains, zircon standards FC1 (1099 Ma; Paces and Miller, 1993) and OD3 (33 Ma; Iwano *et al.*, 2013), and the glass standard NIST SRM610 were mounted in an epoxy resin and polished till the center of the embedded grains exposed in the surface. After polishing, backscattered electron (BSE) and cathodoluminescence (CL) images of the mounted zircons were checked for selecting sites for analysis. For BSE and CL images, a scanning electron microscope-cathodoluminescence equipment, JSM-6610 (JEOL) and a CL detector (Sanyu Electron), was used. U-Pb dating of these samples was carried out using an LA-ICP-MS which constitutes a NWR213 (Elemental Scientific Lasers) and Agilent 7700x (Agilent Technologies) at the National Museum of Nature and Science, Tsukuba, Japan. The experimental conditions and analytical procedures were according to Tsutsumi *et al.* (2012), and additional devices of a buffered type stabilizer (Tunheng and

Hirata, 2004) is applied. The spot size of the laser was 25 μm. A correction for common Pb was made based on the measured ^{207}Pb/^{206}Pb ratio (^{207}Pb correction), and ^{208}Pb/^{206}Pb and Th/U ratios (^{208}Pb correction) (e.g. Williams, 1998) and the model for common Pb compositions proposed by Stacey and Kramers (1975). In this paper, we adopted ^{207}Pb correction for age discussion, since compared with ^{208}Pb correction, it is more effective in calculating Phanerozoic ^{238}U-^{206}Pb* age (e.g. Williams, 1998). ^{208}Pb corrected ^{238}U/^{206}Pb* and ^{207}Pb*/^{206}Pb* ratios were used for drawing a concordia diagram and evaluating whether the data are concordant or discordant because ^{207}Pb correction cannot calculate ^{207}Pb*/^{206}Pb* ratio in principle. Pb* indicates radiometric Pb. The criteria of concordance is that ^{208}Pb corrected ^{207}Pb*/^{206}Pb* with 2σ error overlap of the concordia curve. The pooled ages presented in this study were calculated using IsoplotR software (Vermeesch, 2018). The uncertainties in the weighted mean ^{238}U -^{206}Pb* ages indicate 95% confidence intervals (95% conf.). The data of secondary standard OD3 zircon obtained during analysis yielded weighted mean ages of 32.6 ± 0.7 Ma (n = 6; MSWD = 1.95; when AND1 was analyzed), 33.1 ± 2.3 Ma (n = 4; MSWD = 1.08; when AND2 and AND4 were analyzed) and 32.7 ± 1.3 Ma (n = 5; MSWD = 2.05; when GL18/1 and GL18/2 were analyzed). MSWD is an acronym of mean square weighted deviation, calculated from the square root of the χ^2 value.

Results

Most of the handpicked zircon grains have clear oscillatory zoned texture without any rim, suggesting their igneous origin (Fig. 2C). We analyzed 27 euhedral zircon grains from AND1, 28 from AND2, 29 from AND4, 39 from GL18/1, and 30 from GL18/2, respectively (Fig. 3). Table 1 shows measurements of the secondary standard OD3, and all measurements of zircons in Tables 2–6.

From the sample AND1, 27 spots/grains were analyzed and 26 data were concordant, which range in age from 263.3 ± 4.6 to 235.1 ± 3.7 Ma (Table 2). After two older ages are excluded, the weighted average age of zircon is 247.3 ± 1.7 Ma (one datum is rejected; MSWD = 1.04), i.e., Olenekian, Early
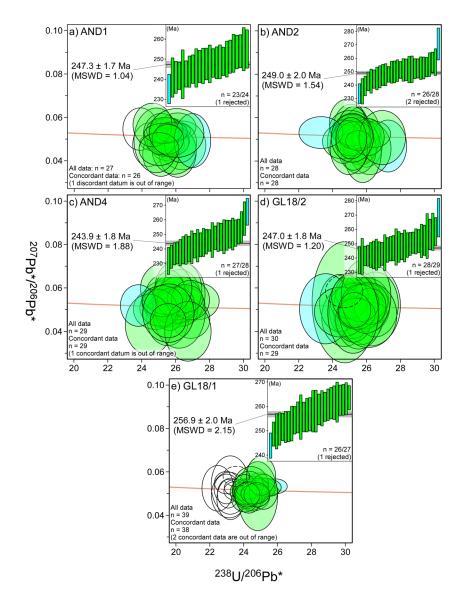
Fig. 3.   Tera-Wasserberg U-Pb concordia diagrams and age distribution plot of zircons from the 5 analyzed samples
from the Andreevka area, SW Primorye. Error ellipses and bars are 95% conf. Solid ellipses: concordant data; bro-
ken ellipses: discordant data; ellipses and bars filled with light green: used for age calculation; ellipses and bard with
blue: rejected for age calculation.

Table 1.   Measurements of U-Pb ages of seconsary
standard zircon (OD3).

date of analysis (yymmdd)	analyzed sample	Age (Ma)	n	MSWD
190612	AND2, AND4	33.1 ± 2.3	4	1.08
191010	AND1	32.6 ± 0.7	6	1.95
201026	GL18/1, GL18/2	32.7 ± 1.3	5	2.05

Age errors are 95% conf.

Triassic (Gradstein *et al.*, 2020; the same time scale
afterwards). From the sample AND2, 28 spots/
grains were analyzed and all data were concordant,
which range in age from 270.6 ± 6.1 to 233.5 ± 3.7 Ma
(Table 3). The weighted average age is 249.0 ± 2.0
Ma (two data are rejected; MSWD = 1.54), i.e., Olenekian,
Early Triassic. From the sample AND4, 29 spots/grains

were analyzed and all data were concordant, which
range in age from 388.8 ± 5.1 to 260.7 ± 5.9 Ma
(Table 4). After one older datum is excluded, the
weighted average age is 243.9 ± 1.8 Ma (one datum
is rejected; MSWD = 1.88), i.e., Anisian, Middle
Triassic. From the sample GL18/2, 30 spots/grains
were analyzed and 29 data were concordant, which
range in age from 268.1 ± 6.9 to 238.3 ± 4.8 Ma
(Table 6). The weighted average age is 247.0 ± 1.8
Ma (one datum is rejected; MSWD = 1.20), i.e.,
Anisian, Middle Triassic. From the sample GL18/1,
39 spots/grains were analyzed and 38 data are con-
cordant, which range in age from 340.0 ± 4.0 to
243.8 ± 2.6 Ma (Table 5). After 11 older ages are
excluded, the weighted average age is 256.9 ± 2.0

Table 2.   Measurements of U-Pb ages of zircons from Sample AND1.

Labels	$^{206}Pb_c$ [1] (%)	U (ppm)	Th (ppm)	Th/U	$^{238}U/^{206}Pb^*$ [1]	$^{207}Pb^*/^{206}Pb^*$ [1]	$^{238}U/^{206}Pb^*$ age [1] (Ma)	$^{238}U/^{206}Pb^*$ age [2] (Ma)	Remarks
AND1_01	0.07	462	185	0.41	25.42 ± 0.38	0.0477 ± 0.0031	248.7 ± 3.7	248.9 ± 3.6	
AND1_02	0.00	305	141	0.47	25.59 ± 0.43	0.0539 ± 0.0024	247.1 ± 4.0	246.3 ± 4.1	
AND1_03	1.00	250	98	0.40	26.40 ± 0.56	0.0471 ± 0.0046	239.6 ± 5.0	240.8 ± 5.0	
AND1_04	0.00	399	226	0.58	26.11 ± 0.44	0.0557 ± 0.0026	242.3 ± 4.0	240.9 ± 4.0	
AND1_05	0.59	256	115	0.46	26.10 ± 0.45	0.0439 ± 0.0047	242.4 ± 4.1	243.8 ± 4.0	
AND1_06	0.00	360	170	0.48	25.45 ± 0.41	0.0540 ± 0.0024	248.4 ± 3.9	247.6 ± 4.0	
AND1_07	0.00	429	150	0.36	24.90 ± 0.42	0.0485 ± 0.0017	253.9 ± 4.2	253.9 ± 4.2	
AND1_08	0.74	391	213	0.56	25.12 ± 0.44	0.0431 ± 0.0042	251.6 ± 4.3	253.5 ± 4.3	
AND1_09	0.00	372	235	0.65	25.48 ± 0.42	0.0474 ± 0.0020	248.1 ± 4.0	248.1 ± 4.0	
AND1_10	0.00	357	203	0.58	36.26 ± 0.88	0.0603 ± 0.0028	175.4 ± 4.2	173.1 ± 4.2	D, N
AND1_11	0.58	246	86	0.36	25.90 ± 0.53	0.0448 ± 0.0045	244.2 ± 4.9	245.6 ± 4.9	
AND1_12	0.00	234	102	0.45	25.65 ± 0.47	0.0491 ± 0.0028	246.6 ± 4.5	246.6 ± 4.5	
AND1_13	0.00	777	383	0.51	25.99 ± 0.36	0.0537 ± 0.0015	243.4 ± 3.3	242.6 ± 3.3	
AND1_14	0.00	264	115	0.45	25.54 ± 0.50	0.0484 ± 0.0027	247.6 ± 4.8	247.6 ± 4.8	
AND1_15	0.25	131	45	0.35	24.85 ± 0.54	0.0494 ± 0.0061	254.3 ± 5.5	254.9 ± 5.5	
AND1_16	1.02	504	302	0.61	26.27 ± 0.39	0.0483 ± 0.0037	240.9 ± 3.5	241.7 ± 3.5	
AND1_17	0.67	357	182	0.52	24.41 ± 0.39	0.0474 ± 0.0041	258.9 ± 4.0	260.2 ± 4.0	N
AND1_18	0.41	319	125	0.40	25.14 ± 0.43	0.0523 ± 0.0039	251.5 ± 4.2	251.2 ± 4.2	N
AND1_19	0.00	384	209	0.56	25.34 ± 0.44	0.0541 ± 0.0024	249.5 ± 4.2	248.6 ± 4.3	
AND1_20	0.03	303	127	0.43	24.62 ± 0.47	0.0565 ± 0.0041	256.6 ± 4.9	255.0 ± 4.9	
AND1_21	0.00	666	189	0.29	25.75 ± 0.38	0.0532 ± 0.0019	245.6 ± 3.6	245.0 ± 3.6	
AND1_22	0.00	388	201	0.53	25.25 ± 0.46	0.0526 ± 0.0019	250.4 ± 4.5	250.0 ± 4.6	
AND1_23	1.13	306	141	0.47	26.98 ± 0.44	0.0493 ± 0.0051	234.6 ± 3.8	235.1 ± 3.7	N
AND1_24	0.20	458	119	0.27	25.53 ± 0.38	0.0499 ± 0.0028	247.7 ± 3.6	248.1 ± 3.6	
AND1_25	0.00	207	80	0.40	25.00 ± 0.48	0.0454 ± 0.0031	252.9 ± 4.8	252.9 ± 4.8	
AND1_26	0.05	313	133	0.44	23.90 ± 0.42	0.0546 ± 0.0040	264.3 ± 4.6	263.3 ± 4.6	
AND1_27	0.00	131	87	0.68	26.04 ± 0.66	0.0528 ± 0.0046	243.0 ± 6.0	242.4 ± 6.2	

Errors are 1-sigma; Pb_c and Pb^* indicate the common and radiogenic portions, respectively.
Remarks; D: discordant, N: not used for weighted mean age calculation
(1) Common Pb corrected by assuming $^{206}Pb/^{238}U$-$^{208}Pb/^{232}Th$ age-concordance
(2) Common Pb corrected by assuming $^{206}Pb/^{238}U$-$^{207}Pb/^{235}U$ age-concordance

Table 3.   Measurements of U-Pb ages of zircons from Sample AND2.

Labels	$^{206}Pb_c$ [1] (%)	U (ppm)	Th (ppm)	Th/U	$^{238}U/^{206}Pb^*$ [1]	$^{207}Pb^*/^{206}Pb^*$ [1]	$^{238}U/^{206}Pb^*$ age [1] (Ma)	$^{238}U/^{206}Pb^*$ age [2] (Ma)	Remarks
AND2_01	1.20	475	283	0.61	25.99 ± 0.38	0.0478 ± 0.0044	243.4 ± 3.5	244.4 ± 3.5	
AND2_02	0.21	232	94	0.42	25.07 ± 0.43	0.0546 ± 0.0047	252.2 ± 4.3	251.1 ± 4.3	
AND2_03	0.80	272	147	0.56	25.68 ± 0.45	0.0519 ± 0.0053	246.3 ± 4.2	246.1 ± 4.2	
AND2_04	0.81	286	114	0.41	25.60 ± 0.44	0.0490 ± 0.0045	247.0 ± 4.2	247.7 ± 4.2	
AND2_05	0.00	304	154	0.52	25.75 ± 0.45	0.0537 ± 0.0025	245.6 ± 4.3	244.8 ± 4.3	
AND2_06	0.13	261	116	0.46	24.84 ± 0.43	0.0576 ± 0.0044	254.5 ± 4.3	252.5 ± 4.3	
AND2_07	0.00	237	102	0.44	24.91 ± 0.36	0.0526 ± 0.0024	253.7 ± 3.6	253.3 ± 3.7	
AND2_08	1.72	223	76	0.35	27.25 ± 0.45	0.0468 ± 0.0049	232.4 ± 3.7	233.5 ± 3.7	N
AND2_09	0.50	195	80	0.42	26.18 ± 0.51	0.0456 ± 0.0049	241.7 ± 4.6	242.9 ± 4.5	
AND2_10	0.00	287	157	0.56	24.95 ± 0.41	0.0535 ± 0.0025	253.3 ± 4.1	252.6 ± 4.2	
AND2_11	0.17	410	210	0.52	25.15 ± 0.33	0.0521 ± 0.0036	251.4 ± 3.2	251.1 ± 3.2	
AND2_12	0.87	255	107	0.43	25.50 ± 0.43	0.0454 ± 0.0046	248.0 ± 4.1	249.7 ± 4.1	
AND2_13	0.75	208	91	0.45	25.75 ± 0.45	0.0439 ± 0.0057	245.6 ± 4.2	247.5 ± 4.0	
AND2_14	0.00	327	157	0.49	26.40 ± 0.41	0.0522 ± 0.0025	239.6 ± 3.6	239.3 ± 3.7	
AND2_15	0.00	231	113	0.50	25.02 ± 0.50	0.0551 ± 0.0033	252.6 ± 4.9	251.5 ± 5.0	
AND2_16	3.57	382	153	0.41	25.20 ± 0.42	0.0503 ± 0.0060	250.9 ± 4.1	251.2 ± 4.1	
AND2_17	0.02	309	127	0.42	24.60 ± 0.38	0.0488 ± 0.0041	256.9 ± 3.9	257.0 ± 3.8	
AND2_18	0.00	214	97	0.47	24.58 ± 0.49	0.0489 ± 0.0033	257.0 ± 5.1	257.0 ± 5.1	
AND2_19	0.00	440	154	0.36	25.07 ± 0.38	0.0475 ± 0.0021	252.1 ± 3.8	252.1 ± 3.8	
AND2_20	0.40	486	205	0.43	26.07 ± 0.39	0.0509 ± 0.0035	242.6 ± 3.5	242.7 ± 3.5	
AND2_21	0.00	267	108	0.42	25.14 ± 0.41	0.0541 ± 0.0030	251.5 ± 4.0	250.6 ± 4.1	
AND2_22	1.02	300	170	0.58	24.93 ± 0.45	0.0461 ± 0.0051	253.5 ± 4.5	255.2 ± 4.5	
AND2_23	0.00	237	123	0.53	23.29 ± 0.53	0.0530 ± 0.0030	271.0 ± 6.0	270.6 ± 6.1	N
AND2_24	0.00	322	150	0.48	25.32 ± 0.42	0.0517 ± 0.0026	249.7 ± 4.1	249.5 ± 4.2	
AND2_25	0.00	476	208	0.45	25.51 ± 0.31	0.0492 ± 0.0019	247.9 ± 3.0	247.9 ± 3.0	
AND2_26	0.18	190	74	0.40	26.91 ± 0.56	0.0507 ± 0.0051	235.2 ± 4.8	235.2 ± 4.8	
AND2_27	0.37	240	81	0.35	25.14 ± 0.51	0.0506 ± 0.0046	251.5 ± 5.0	251.7 ± 5.0	
AND2_28	0.14	358	169	0.49	25.08 ± 0.37	0.0504 ± 0.0039	252.0 ± 3.7	252.3 ± 3.7	

Errors are 1-sigma; Pb_c and Pb^* indicate the common and radiogenic portions, respectively.
Remarks; D: discordant, N: not used for weighted mean age calculation
(1) Common Pb corrected by assuming $^{206}Pb/^{238}U$-$^{208}Pb/^{232}Th$ age-concordance
(2) Common Pb corrected by assuming $^{206}Pb/^{238}U$-$^{207}Pb/^{235}U$ age-concordance

Table 4.   Measurements of U-Pb ages of zircons from Sample AND4.

Labels	$^{206}Pb_c$ [1] (%)	U (ppm)	Th (ppm)	Th/U	$^{238}U/^{206}Pb^*$ [1]	$^{207}Pb^*/^{206}Pb^*$ [1]	$^{238}U/^{206}Pb^*$ age [1] (Ma)	$^{238}U/^{206}Pb^*$ age [2] (Ma)	Remarks
AND4_01	0.00	232	93	0.41	27.21 ± 0.55	0.0538 ± 0.0035	232.6 ± 4.6	231.8 ± 4.7	
AND4_02	0.00	230	131	0.58	25.27 ± 0.53	0.0538 ± 0.0038	250.2 ± 5.1	249.4 ± 5.3	
AND4_03	0.48	400	222	0.57	26.88 ± 0.46	0.0455 ± 0.0036	235.5 ± 3.9	236.6 ± 3.9	
AND4_04	0.03	184	80	0.45	25.40 ± 0.52	0.0541 ± 0.0051	248.9 ± 5.0	248.0 ± 5.0	
AND4_05	0.00	197	79	0.41	25.27 ± 0.57	0.0507 ± 0.0037	250.2 ± 5.6	250.2 ± 5.6	
AND4_06	0.09	234	103	0.45	26.22 ± 0.50	0.0559 ± 0.0051	241.3 ± 4.5	239.9 ± 4.5	
AND4_07	0.02	337	179	0.55	25.71 ± 0.46	0.0544 ± 0.0047	245.9 ± 4.4	245.0 ± 4.3	
AND4_08	0.00	165	47	0.29	26.20 ± 0.62	0.0523 ± 0.0035	241.5 ± 5.6	241.1 ± 5.7	
AND4_09	0.03	164	74	0.46	26.45 ± 0.52	0.0570 ± 0.0059	239.2 ± 4.7	237.4 ± 4.6	
AND4_10	0.00	323	155	0.49	25.16 ± 0.47	0.0525 ± 0.0027	251.2 ± 4.6	250.8 ± 4.6	
AND4_11	0.00	237	115	0.50	26.12 ± 0.48	0.0492 ± 0.0030	242.2 ± 4.3	242.2 ± 4.3	
AND4_12	0.20	222	99	0.46	25.52 ± 0.51	0.0463 ± 0.0053	247.8 ± 4.9	248.3 ± 4.7	
AND4_13	0.60	144	44	0.31	26.19 ± 0.63	0.0488 ± 0.0068	241.5 ± 5.7	242.2 ± 5.7	
AND4_14	0.00	305	158	0.53	25.88 ± 0.53	0.0507 ± 0.0029	244.4 ± 4.9	244.4 ± 4.9	
AND4_15	0.01	211	85	0.41	26.14 ± 0.57	0.0590 ± 0.0056	242.0 ± 5.2	239.6 ± 5.2	
AND4_16	0.00	514	310	0.62	16.02 ± 0.21	0.0581 ± 0.0019	390.4 ± 5.0	388.7 ± 5.1	N
AND4_17	1.96	464	258	0.57	25.64 ± 0.40	0.0542 ± 0.0057	246.7 ± 3.8	245.8 ± 3.8	
AND4_18	0.00	335	132	0.41	25.10 ± 0.44	0.0480 ± 0.0023	251.9 ± 4.4	251.9 ± 4.4	
AND4_19	0.00	378	216	0.59	25.97 ± 0.45	0.0536 ± 0.0027	243.6 ± 4.1	242.8 ± 4.2	
AND4_20	0.00	546	300	0.56	26.54 ± 0.43	0.0550 ± 0.0026	238.4 ± 3.8	237.2 ± 3.8	
AND4_21	0.00	249	124	0.51	26.86 ± 0.46	0.0543 ± 0.0037	235.6 ± 3.9	234.6 ± 4.1	
AND4_22	0.00	182	52	0.29	24.79 ± 0.53	0.0501 ± 0.0038	254.9 ± 5.4	254.9 ± 5.4	
AND4_23	0.00	130	39	0.30	25.43 ± 0.62	0.0597 ± 0.0049	248.7 ± 6.0	246.1 ± 6.1	
AND4_24	0.74	157	48	0.32	24.41 ± 0.57	0.0430 ± 0.0057	258.8 ± 6.0	260.7 ± 5.9	
AND4_25	0.05	274	71	0.26	23.78 ± 0.43	0.0518 ± 0.0039	265.5 ± 4.7	265.4 ± 4.7	
AND4_26	0.00	283	144	0.52	25.20 ± 0.49	0.0538 ± 0.0029	250.9 ± 4.8	250.1 ± 4.9	
AND4_27	0.91	196	58	0.30	26.71 ± 0.56	0.0399 ± 0.0056	236.9 ± 4.8	239.1 ± 4.8	
AND4_28	0.62	182	54	0.30	25.56 ± 0.62	0.0483 ± 0.0055	247.4 ± 5.9	248.3 ± 5.9	
AND4_29	0.00	245	57	0.24	25.54 ± 0.43	0.0448 ± 0.0032	247.6 ± 4.1	247.6 ± 4.1	

Errors are 1-sigma; Pb_c and Pb^* indicate the common and radiogenic portions, respectively.
Remarks; D: discordant, N: not used for weighted mean age calculation
(1) Common Pb corrected by assuming $^{206}Pb/^{238}U$-$^{208}Pb/^{232}Th$ age-concordance
(2) Common Pb corrected by assuming $^{206}Pb/^{238}U$-$^{207}Pb/^{235}U$ age-concordance

Ma (one datum is rejected; MSWD = 2.15), i.e., Wuchiapingian, Late Permian.

These results clarified that the five granitoid samples (one quartz diorite, three granodiorite, and one granite) from the Gamov intrusions have igneous ages that range in 257–244 Ma; i.e., Wuchiapingian (Permian) to Anisian (Triassic). The older part of this age range overlaps with the previously reported zircon ages of 259 and 254 Ma (Wuchiapingian-Changhsingian, Permian) from the granitoids in the Andreevka area, ca. 8 km to the southeast from the locality of AND2 (Kruk *et al.*, 2015; Fig. 1B). The present study results indicate that the Gamov intrusion has formed during the late Permian-Middle Triassic.

Discussion

Triassic granitoids in the LG belt: Among the analyzed five granitoid samples from the Gamov intrusions, four samples were previously assigned to the Permian, and the rest one to the Jurassic, based on the biotite/amphibole K-Ar dating (SGM). The present study, however, identified for the first time the Early-Middle Triassic zircon U-Pb ages from the granitoids of the Gamov intrusions in the easternmost LG belt, southern Primorye. Furthermore, one Permian age was confirmed for the Gamov intrusions, in addition to the two ages reported previously from different localities by Kruk *et al.* (2015) (Fig. 1B). As to the Gamov intrusions, therefore, the available seven ages prove that the granitoids are products of magmatism during the late Permian to Middle Triassic interval. The previously claimed Jurassic granitoids (SGM) have not yet been confirmed in the study area.

Our results suggest that the potentially larger extent of Triassic granitoids throughout the LG belt than previously believed. The sporadic occurrence of the Permo-Triassic granitoids and coeval felsic volcanic rocks were lately reported not only from the northern parts of the LG belt in Primorye (Khanchuk *et al.*, 2010; Golozubov *et al.*, 2017; Chashchin *et al.*, 2020) but also from the Popov and Russky islands on the southwest of Vladivostok, near the boundary to the Khanka block (Tsutsumi *et*

Table 5.   Measurements of U-Pb ages of zircons from Sample GL18/1.

Labels	$^{206}Pb_c^{(1)}$ (%)	U (ppm)	Th (ppm)	Th/U	$^{238}U/^{206}Pb^{*(1)}$	$^{207}Pb^{*}/^{206}Pb^{*(1)}$	$^{238}U\text{-}^{206}Pb^{*}$ age $^{(1)}$ (Ma)	$^{238}U\text{-}^{206}Pb^{*}$ age $^{(2)}$ (Ma)	Remarks
GL18/1_001	0.00	378	135	0.37	25.08 ± 0.32	0.0525 ± 0.0019	252.0 ± 3.1	251.6 ± 3.2	
GL18/1_002	0.00	1164	1004	0.88	25.44 ± 0.26	0.0510 ± 0.0010	248.6 ± 2.5	248.6 ± 2.5	
GL18/1_003	0.00	618	270	0.45	25.13 ± 0.29	0.0516 ± 0.0015	251.6 ± 2.8	251.5 ± 2.8	
GL18/1_004	0.00	361	221	0.63	23.55 ± 0.32	0.0578 ± 0.0019	268.0 ± 3.6	266.0 ± 3.6	D, N
GL18/1_005	0.00	429	248	0.59	23.55 ± 0.29	0.0526 ± 0.0016	268.1 ± 3.3	267.8 ± 3.3	N
GL18/1_006	0.51	174	80	0.47	23.21 ± 0.33	0.0474 ± 0.0039	271.9 ± 3.8	273.3 ± 3.7	N
GL18/1_007	0.00	879	515	0.60	25.87 ± 0.28	0.0532 ± 0.0014	244.5 ± 2.6	243.8 ± 2.6	N
GL18/1_008	0.00	744	395	0.54	23.97 ± 0.24	0.0504 ± 0.0011	263.5 ± 2.5	263.5 ± 2.5	
GL18/1_009	0.00	608	738	1.25	24.86 ± 0.29	0.0499 ± 0.0016	254.3 ± 2.9	254.3 ± 2.9	
GL18/1_010	0.00	519	236	0.47	24.28 ± 0.29	0.0529 ± 0.0015	260.2 ± 3.0	259.8 ± 3.1	
GL18/1_011	0.00	140	81	0.59	24.49 ± 0.42	0.0484 ± 0.0027	258.0 ± 4.4	258.0 ± 4.4	
GL18/1_012	0.06	457	229	0.51	24.44 ± 0.32	0.0490 ± 0.0028	258.6 ± 3.3	258.7 ± 3.2	
GL18/1_013	0.35	119	78	0.67	24.81 ± 0.48	0.0487 ± 0.0065	254.7 ± 4.8	255.6 ± 4.6	
GL18/1_014	0.00	445	221	0.51	18.46 ± 0.23	0.0506 ± 0.0015	340.0 ± 4.0	340.0 ± 4.0	N
GL18/1_015	0.00	651	584	0.92	25.27 ± 0.38	0.0527 ± 0.0017	250.2 ± 3.7	249.7 ± 3.7	
GL18/1_016	0.09	420	200	0.49	24.18 ± 0.34	0.0496 ± 0.0027	261.3 ± 3.6	261.5 ± 3.5	
GL18/1_017	0.11	411	199	0.50	24.62 ± 0.34	0.0514 ± 0.0026	256.7 ± 3.5	256.7 ± 3.5	
GL18/1_018	0.16	428	132	0.32	24.05 ± 0.32	0.0473 ± 0.0024	262.6 ± 3.4	263.0 ± 3.4	
GL18/1_019	0.00	253	85	0.35	22.97 ± 0.29	0.0549 ± 0.0021	274.7 ± 3.4	273.7 ± 3.5	N
GL18/1_020	0.00	184	153	0.85	24.14 ± 0.39	0.0506 ± 0.0025	261.7 ± 4.2	261.7 ± 4.2	
GL18/1_021	0.00	395	387	1.01	23.55 ± 0.30	0.0511 ± 0.0018	268.1 ± 3.3	268.1 ± 3.3	N
GL18/1_022	0.59	596	333	0.57	23.07 ± 0.26	0.0498 ± 0.0027	273.6 ± 3.1	274.2 ± 3.0	N
GL18/1_023	0.01	894	497	0.57	18.76 ± 0.20	0.0515 ± 0.0019	334.8 ± 3.4	334.8 ± 3.4	N
GL18/1_024	0.11	381	135	0.36	22.97 ± 0.30	0.0520 ± 0.0028	274.7 ± 3.6	274.6 ± 3.6	N
GL18/1_025	0.00	411	155	0.39	24.06 ± 0.30	0.0509 ± 0.0018	262.5 ± 3.2	262.5 ± 3.2	
GL18/1_026	0.08	243	84	0.36	24.43 ± 0.42	0.0535 ± 0.0036	258.6 ± 4.3	257.9 ± 4.3	
GL18/1_027	0.00	429	205	0.49	24.69 ± 0.32	0.0530 ± 0.0016	255.9 ± 3.2	255.4 ± 3.3	
GL18/1_028	0.00	223	147	0.68	24.31 ± 0.34	0.0538 ± 0.0026	259.9 ± 3.6	259.2 ± 3.7	
GL18/1_029	0.27	148	64	0.44	23.13 ± 0.43	0.0492 ± 0.0043	272.8 ± 4.9	273.5 ± 4.8	N
GL18/1_030	1.31	138	79	0.58	23.19 ± 0.46	0.0538 ± 0.0055	272.1 ± 5.3	271.5 ± 5.2	N
GL18/1_031	0.25	475	189	0.41	24.04 ± 0.30	0.0518 ± 0.0028	262.7 ± 3.3	262.7 ± 3.2	
GL18/1_032	0.18	378	179	0.49	24.28 ± 0.32	0.0482 ± 0.0030	260.2 ± 3.4	260.6 ± 3.3	
GL18/1_033	0.32	396	216	0.56	25.15 ± 0.34	0.0507 ± 0.0033	251.3 ± 3.3	251.5 ± 3.3	
GL18/1_034	0.00	309	100	0.33	24.65 ± 0.34	0.0497 ± 0.0019	256.3 ± 3.5	256.3 ± 3.5	
GL18/1_035	0.43	384	280	0.75	25.01 ± 0.35	0.0580 ± 0.0037	252.7 ± 3.5	250.7 ± 3.4	
GL18/1_036	1.19	213	81	0.39	22.45 ± 0.38	0.0523 ± 0.0043	281.0 ± 4.7	280.8 ± 4.6	N
GL18/1_037	0.14	514	162	0.32	24.76 ± 0.31	0.0493 ± 0.0023	255.2 ± 3.1	255.6 ± 3.1	
GL18/1_038	0.02	532	214	0.41	24.18 ± 0.31	0.0493 ± 0.0023	261.2 ± 3.3	261.3 ± 3.3	
GL18/1_039	0.00	277	96	0.36	24.93 ± 0.36	0.0535 ± 0.0024	253.6 ± 3.6	252.9 ± 3.6	

Errors are 1-sigma; Pb_c and Pb^{*} indicate the common and radiogenic portions, respectively.
Remarks; D: discordant, N: not used for weighted mean age calculation
(1) Common Pb corrected by assuming $^{206}Pb/^{238}U$-$^{208}Pb/^{232}Th$ age-concordance
(2) Common Pb corrected by assuming $^{206}Pb/^{238}U$-$^{207}Pb/^{235}U$ age-concordance

al., 2014; S'edin et al., 2018; Fig. 1A). Furthermore in west-neighboring Jilin/Heilongjiang, China, intense U-Pb dating for granitoids of the LG belt revealed age of 280-233 Ma (early Permian to mid-Triassic; Ma et al., 2016; Chen et al., 2017). These results lead us to conclude that that the Permo-Triassic igneous rocks in the LG belt, including the Gamov intrusions, were generated not as small-scale isolated plutons but primarily formed parts of a much larger batholith belt that developed probably on the over 100 km-scale.

The pre-Cretaceous LG belt is fundamentally characterized by the Permian-Triassic and Jurassic granitoids (Fig. 1A), whereas the pre-Cretaceous Khanka block on the east features solely Paleozoic granitoids (Nevolin et al., 2012) without Triassic and Jurassic ones. Thus, the Permo-Triassic extensive felsic magmatism in the eastern LG belt (Andreevka area and Russky/Popov islands) highlights a sharp contrast to the Khanka block on the east, particularly in ages of granitoids. In this regard, the West Primorye fault in southwestern Primorye (Fig. 1A) unlikely represent the boundary between the two distinct granitoid provinces, particularly the eastern limit for the Permo-Triassic and Jurassic granitoids. Instead, the boundary of the two granitoid provinces is traced, from north to south, probably along the western coast of the Khanka Lake (Khanchuk et al., 2010; Chashchin et al., 2020), between the Russky Island and Vladivostok (Tsutsumi et al., 2014; S'edin et al., 2018), and offshore the eastern Gamov peninsula (Kruk et al., 2015; this study) (Fig. 1A).

Age constraints to host Paleozoic strata: The host unit for the Permo-Triassic Gamov granitoids in the Andreevka area comprises the "Permian" ter-

Table 6. Measurements of U-Pb ages of zircons from Sample GL18/2.

Labels	$^{206}Pb_c^{(1)}$ (%)	U (ppm)	Th (ppm)	Th/U	$^{238}U/^{206}Pb^{*\,(1)}$	$^{207}Pb^*/^{206}Pb^{*\,(1)}$	$^{238}U\text{-}^{206}Pb^*$ age $^{(1)}$ (Ma)	$^{238}U\text{-}^{206}Pb^*$ age $^{(2)}$ (Ma)	Remarks
GL18/2_001	3.00	53	20	0.39	24.70 ± 0.79	0.0533 ± 0.0114	255.8 ± 8.0	255.3 ± 8.0	
GL18/2_002	0.51	71	31	0.45	26.22 ± 0.72	0.0518 ± 0.0076	241.3 ± 6.5	241.0 ± 6.4	
GL18/2_003	0.00	136	80	0.60	25.76 ± 0.47	0.0479 ± 0.0030	245.5 ± 4.4	245.5 ± 4.4	
GL18/2_004	0.00	108	54	0.52	26.02 ± 0.52	0.0544 ± 0.0041	243.1 ± 4.8	242.1 ± 4.9	
GL18/2_005	0.12	84	34	0.42	24.68 ± 0.55	0.0464 ± 0.0055	256.1 ± 5.6	256.4 ± 5.4	
GL18/2_006	0.52	87	34	0.40	25.63 ± 0.57	0.0480 ± 0.0058	246.7 ± 5.4	247.6 ± 5.4	
GL18/2_007	0.00	155	92	0.61	24.66 ± 0.45	0.0583 ± 0.0031	256.3 ± 4.6	254.1 ± 4.6	D, N
GL18/2_008	0.28	161	64	0.41	26.12 ± 0.50	0.0510 ± 0.0046	242.2 ± 4.6	242.2 ± 4.6	
GL18/2_009	0.45	117	43	0.38	25.11 ± 0.54	0.0495 ± 0.0053	251.8 ± 5.4	252.3 ± 5.4	
GL18/2_010	0.42	129	66	0.53	24.41 ± 0.49	0.0529 ± 0.0054	258.8 ± 5.1	258.4 ± 5.0	
GL18/2_011	1.00	74	32	0.44	25.51 ± 0.60	0.0496 ± 0.0073	247.8 ± 5.7	248.3 ± 5.7	
GL18/2_012	0.00	162	95	0.60	25.63 ± 0.47	0.0471 ± 0.0026	246.8 ± 4.5	246.8 ± 4.5	
GL18/2_013	0.00	133	72	0.55	25.31 ± 0.48	0.0575 ± 0.0036	249.8 ± 4.6	247.9 ± 4.7	
GL18/2_014	0.00	70	31	0.45	25.49 ± 0.67	0.0526 ± 0.0039	248.0 ± 6.4	247.6 ± 6.5	
GL18/2_015	0.00	194	106	0.56	26.06 ± 0.45	0.0501 ± 0.0027	242.8 ± 4.1	242.8 ± 4.1	
GL18/2_016	0.00	154	70	0.47	26.06 ± 0.48	0.0536 ± 0.0033	242.8 ± 4.3	242.0 ± 4.4	
GL18/2_017	0.11	71	28	0.40	23.57 ± 0.63	0.0503 ± 0.0066	267.8 ± 7.0	268.1 ± 6.9	N
GL18/2_018	0.43	217	121	0.57	25.21 ± 0.43	0.0455 ± 0.0043	250.7 ± 4.2	251.8 ± 4.1	
GL18/2_019	0.00	278	133	0.49	26.19 ± 0.41	0.0482 ± 0.0021	241.6 ± 3.7	241.6 ± 3.7	
GL18/2_020	0.00	65	29	0.45	24.47 ± 0.64	0.0488 ± 0.0047	258.2 ± 6.6	258.2 ± 6.6	
GL18/2_021	0.62	128	65	0.52	26.51 ± 0.55	0.0523 ± 0.0061	238.7 ± 4.8	238.3 ± 4.8	
GL18/2_022	0.00	228	107	0.48	25.31 ± 0.42	0.0490 ± 0.0027	249.8 ± 4.1	249.8 ± 4.1	
GL18/2_023	0.00	118	65	0.56	25.00 ± 0.44	0.0556 ± 0.0041	252.8 ± 4.3	251.5 ± 4.5	
GL18/2_024	0.55	104	39	0.38	26.08 ± 0.69	0.0474 ± 0.0061	242.5 ± 6.3	243.6 ± 6.4	
GL18/2_025	0.35	278	117	0.43	26.20 ± 0.38	0.0514 ± 0.0034	241.5 ± 3.4	241.4 ± 3.4	
GL18/2_026	0.00	162	92	0.58	25.61 ± 0.45	0.0529 ± 0.0035	247.0 ± 4.2	246.4 ± 4.4	
GL18/2_027	0.00	153	98	0.65	25.39 ± 0.45	0.0480 ± 0.0029	249.0 ± 4.4	249.0 ± 4.4	
GL18/2_028	0.23	110	62	0.58	25.95 ± 0.60	0.0561 ± 0.0070	243.7 ± 5.5	242.2 ± 5.5	
GL18/2_029	0.19	288	96	0.34	25.27 ± 0.39	0.0497 ± 0.0033	250.2 ± 3.8	250.6 ± 3.8	
GL18/2_030	0.90	95	51	0.55	25.19 ± 0.61	0.0484 ± 0.0076	251.0 ± 6.0	251.8 ± 5.9	

Errors are 1-sigma; Pb_c and Pb^* indicate the common and radiogenic portions, respectively.
Remarks; D: discordant, N: not used for weighted mean age calculation
(1) Common Pb corrected by assuming $^{206}Pb/^{238}U\text{-}^{208}Pb/^{232}Th$ age-concordance
(2) Common Pb corrected by assuming $^{206}Pb/^{238}U\text{-}^{207}Pb/^{235}U$ age-concordance

rigenous clastics called the Reshetnikov Fm. The sandstones and mudstones of the formation regionally suffered contact metamorphism by the Permo-Triassic Gamov granitoids, i.e., partly baked up into hornfels. The sporadic occurrence of plant fossils suggested that this formation can be correlated with non-marine/shallow marine Permian (SGM); however, age constraints by Permo-Triassic plant fossils are still loose (Du *et al.*, 2021), and no other direct age indicator has been available. Under the circumstances, the Triassic age of the GL18/2 granitoid near the contact to the Reshetnikov Fm (Fig. 1B) limits the possible depositional age for the Reshetnikov Fm to pre-244 Ma (Anisian or older).

This is concordant with the previously reported fossil ages from the western extension of the Reshetnikov Fm in the Hamgyong-Buk and Jilin. The Tuman System along the Tumangan River in the China/N. Korea border zone is composed of ca. 4,000 m-thick terrigenous clastics with some intercalations of limestone, and felsic/mafic volcanics (Noda, 1958; Lee, 1987; Paek *et al.*, 1993). Fossils reported from the Tuman System include late Car-

boniferous corals, crinoids, brachiopods and middle Permian (273–260 Ma) fusulines, brachiopods, crinoids, and land plants (Noda, 1958; Huang, 1991; Paek *et al.*, 1993). Thus the correlation of the Reshetnikov Fm in the Andreevka area with the upper part of the Tuman System in Hamgyong-Buk and Jilin appears reasonable, and the upper part of the thick formation may range up to Lower Triassic.

Possible link to the Hida belt in Japan: In regard of the correlation between Primorye and Japan, pre-Cretaceous granitoids of the Hida belt in central Japan (Fig. 4) are particularly noteworthy. The Hida belt is characterized by two stages of granitic magmatism; i.e., first in the Permian-Triassic (ca. 250–235 Ma) and the second in the Jurassic (ca. 200–190 Ma) (e.g. Soma *et al.*, 1990; Kano, 1990; Kunugiza *et al.*, 2010; Takahashi *et al.*, 2010, 2018; Horie *et al.*, 2010, 2018; Zhao *et al.*, 2013; Takehara and Horie, 2019).

The origin of the Hida belt has been discussed mostly in view of the primary connection to the North China block that features extensive Archean-Proterozoic basements together with marginal tec-
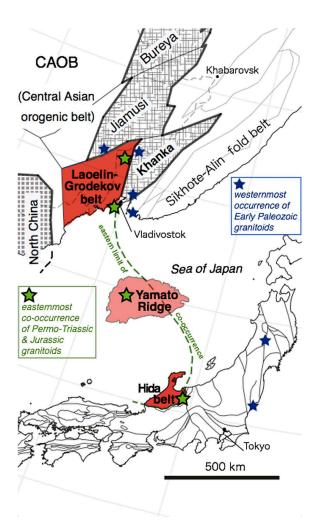
Fig. 4. Geotectonic map of the circum-Sea of Japan, East Asia (compiled from Khanchuk *et al.*, 1996; Wilde, 2015; Isozaki *et al.*, 2010), showing relative positions of the LG belt in Primorye, the Yamato ridge in the middle of the Sea of Japan, and the Hida belt in central Japan. Green stars represent the easternmost (Pacific-side) localities of co-occurred Permo-Triassic and Jurassic granitoids in the LG belt, Yamato Ridge, and Hida belt (Ma *et al.*, 2014; Lelikov *et al.*, 1996), and blue ones the westernmost locality of Early Paleozoic granitoids on the Pacific side (Sakashima *et al.*, 2003; Tagiri *et al.*, 2011; Kruk *et al.*, 2012; Isozaki *et al.*, 2015). The geologic similarities, particularly in the two-fold granitoid ages of the Permo-Triassic and Jurassic, suggest the primary consanguinity among the LG belt, Yamato Ridge, and Hida belt, although they have been separated from each other since the Miocene opening of the Sea of Japan. Note that the Hida belt can be correlated neither with North China block nor Khanka block but uniquely to the LG belt.

tonic zones, i.e., the Ogchon and Imjingan belts, in the Korean peninsula (e.g. Hiroi, 1981; Soma *et al.*, 1990; Oh, 2006). On the other hand, some researchers tried to correlate the Hida belt with the Khanka

block (e.g. Zonenshain *et al.*, 1990). These traditional views were mostly based on the physiological proximity, the occurrence of similar rock types in nearby ages, and also the long-time belief on assumed Precambrian basement. Regional and geochronological studies during the last decade, however, confirmed the absence of Precambrian basement in the Hida belt; namely the oldest unit ever identified is indeed no older than the middle Permian (ca. 270 Ma; Takahashi *et al.*, 2018) except for inherited Precambrian zircons dated up to the early Archean (Horie *et al.*, 2010).

On the other hand, as emphasized by Jahn (2000) and Arakawa *et al.* (2000), the trace element geochemistry of the Hida granitoids is totally different from other Phanerozoic granitoids in Japan essentially formed under ancient Pacific (Panthalassan) subduction settings (e.g. Jahn *et al.*, 2000). This geochemical uniqueness of the Hida granitoids positively supports the allochthoneity of the Hida belt with respect to the rest of the Phanerozoic crusts in Japan (Soma *et al.*, 1990; Isozaki, 1996). It is further noteworthy that the Nd and Sr isotopic signatures of the Hida granitoids and gneisses refute all the previous correlations directly with the North China block *per se*, instead, suggests a possible link to CAOB developed on the north of the North China block (Jahn, 2000; Arakawa *et al.*, 2000; Fig. 4).

The co-occurrence of Permo-Triassic and Jurassic granitoids is regionally identified in the LG belt, as confirmed not only in Primorye (Tsutsumi *et al.*, 2014; S'edin *et al.*, 2018; this study) but also in Jilin (Ma et al, 2014; Chen *et al.*, 2017) and Hamgyong-Buk (Zhai *et al.*, 2016). Among them, the granitoids on the Russky and Popov islands in the Bay of Peter the Great (Fig. 1A) mark the eastern limit for their co-occurrence in Far East Russia. The Hida belt in Japan (Fig. 4) likewise marks the Pacific-side limit of the co-occurrence of the Permo-Triassic and Jurassic granitoids in Japan, suggesting a similar geotectonic setting to the LG belt. These suggest that the Hida belt is correlated neither with the North China block nor the Khanka block as previously claimed, but uniquely with the LG belt.

Although the Hida belt and the coastal LG belt in the mainland Asia are currently separated for nearly 1,000 km in N-S direction, there is a good candidate for a mid-way connecting reference between the LG

and Hida belts, i.e. the Yamato Ridge in the midst of the Sea of Japan (Fig. 4) forming a prominent submarine topographic relief over 200 km wide in E-W direction. The most critical clue for correlation from the Yamato Ridge is the occurrence both of Permo-Triassic (270–222 Ma) and Jurassic (194–152 Ma) granitoids (Ueno *et al.*, 1974; Kaneoka *et al.*, 1996; Lelikov and Malyarenko, 1994; Lelikov *et al.*, 1996; Lelikov and Pugachev, 2016) with uniquely high Sr/Sr ratio of 0.7043 (Ueno *et al.*, 1974), which corresponds to that detected in the Hida granitoids (Shibata *et al.*, 1970). These strongly support the pre-Miocene consanguinity among the above three geotectonic domains currently separated from each other in great distances. The claimed Hida-Yamato Ridge-LG belt connection provides an alternative correlation scheme for the pre-Miocene paleogeography between the mainland Asia and Japan.

In accordance with the proposed geotectonic framework (Fig. 4), the Early Paleozoic granitoids identified in Japan all occur on the Pacific side of the Hida belt (Sakashima *et al.*, 2003; Tagiri *et al.*, 2011; Isozaki *et al.*, 2015), which are fairly correlated with those in the Khanka block and Sergeevka belt on the Pacific side of the LG belt (Isozaki *et al.*, 2017). In southern Primorye, therefore, the boundary between the LG belt and Khanka block is represented unlikely by the putative West Primorye fault but by another tectonic line that runs likely from western Khanka Lake, via Vladivostok/Russky Island strait, to the eastern off-shore of the Gamov peninsula (Fig. 1A). Thus the LG belt in Primorye, the Yamato ridge, and the Hida belt in Japan altogether demonstrate a prominent eastern limit of the associated occurrence of Permo-Triassic and Jurassic granitoids in Far East Asia (Fig. 4), probably suggesting the existence of a major geotectonic boundary that possibly represents the western margin of GSC (Isozaki, 2019).

Conclusions

We conducted zircon U-Pb dating for arc-type granitoids in the eastern LG belt in southwestern Primorye, Far East Russia, by LA-ICPMS. The following results were obtained.

1) Five granitoids of the Gamov intrusions in the Andreevka area, southwestern Primorye, along the Sea of Japan, yielded four ages of the Early-Middle Triassic and one late Permian age.

2) These ages prove the extensive occurrence of the Permo-Triassic granitoids in the LG belt in Primorye, as well as in Jilin (China) and Hamgyong-Buk (North Korea), which primarily formed large-scale arc batholiths.

3) The co-occurrence of the Permo-Triassic and Jurassic granitoids positively suggests the correlation and continuity among the LG belt in mainland Asia, Yamato ridge in the middle of the Sea of Japan, and the Hida belt in central Japan before the Miocene opening of the back-arc basin. This connection may provide a prime clue for pelaogeographical reconstruction of the pre-Sea of Japan Far East Asia.

References

Arakawa, Y., Saito, Y. and Amakawa, H. (2000) Crustal development of the Hida belt, Japan: evidence from Nd-Sr isotopic and chemical characteristics of igneous and metamorphic rocks. *Tectonophysics* **328**: 183–204.

Cao, H.H. Xu, W.L., Pei, F.P. and Zhang, X.Z. (2011) Permian tectonic evolution on southwestern Khanka massif: evidence from zircon U-Pb chronology, Hf isotope and geochemistry of gabbro and diorite. *Acta Geologica Sinica*, **85**: 1390-1402.

Chashchin A.A., Chashchin S.A., Kasatkin S.A. and Golozubov V.V., (2020) Late Triassic volcanic rocks of Talminsky complex (southwestern Primorye): Mineralogy, geochemistry and genesis. *Advance in Current Natural Sciences*, **11**: 139–148 (in Russian).

Chen, C., Ren, Y.S., Zhao, H.L., Yang, Q. and Shang, Q.Q. (2017) Age, tectonic setting, and metallogenic implication of Phanerozoic granitic magmatism at the easterm margin of the Xing'an-Mongolian orogenic belt, NE China. *Journal of Asian Earth Sciences*, **144**: 3688–383.

Cluzel, D., Lee, B.J., and Cadet, J.P. (1991) Indosinian dextral ductile fault system and synkinematic plutonism in the southwest of the Ogcheon belt (South Korea). *Tectonophysics*, **194**: 131–151.

Du, Q.X., Li, G.S., Han, Z.Z. and Shen, X.L. (2021) Reap-

praisal of ages of Triassic continental sedimentary successions in the Yanbian area (NE China): implications for the Triassic Angaran and Cathaysian floral recovery. *Journal of Asian Earth Sciences*, **215**: 104811.

Ehiro, M. (2001) Origins and drift histories of some microcontinents distributed in the eastern margin of Asian continent. *Earth Science (Chikyu-Kagaku)*, **55**: 71–81 (in Japanese with English abstract).

Golozubov, V.V. and Khanchuk, A.I. (2021) The Heilongjiang complex as a fragment of a Jurassic accretionary wedge in the tectonic windows of the overlying plate: A flat slab subduction model. *Russian Journal of Pacific Geology*, **15**: 279–292.

Golozubov V.V., Kruk N.N., Kiselyov V.I., Kasatkin S.A., Rudnev S.N. and Kruk E.A. (2017) First evidence for the Middle Triassic volcanism in South Primorye. *Russian Journal Pacific Geology*, **11**: 110–122.

Golozubov, V.V. and Simanenko, L.F. (2021) Tectonostratigraphy of the Jurassic accretionary prisms in the Sikhote-Alin region of Russian Far East. *Scientific Reports*, **11**: 19337.

Hiroi, Y. (1981) Subdivision of the Hida metamorphic complex, central Japan, and its bearing on the geology of the Far East in pre-Sea of Japan time. *Tectonophysics*, **76**, 317–333.

Horie, K., Ymashita, M., Hayasaka, Y., Katoh, Y., Tsutsumi, Y., Katsube, A., Hidaka, H., Kim, H.C. and Cho, M.S. (2010) Eoarchean–Paleoproterozoic zircon inheritance in Japanese Permo-Triassic granites (Unazuki area, Hida Metamorphic Complex): Unearthing more old crust and identifying source terrranes. *Precambrian Research*, **183**: 145–157.

Horie, K., Tsutsumi, Y., Takehara, M. and Hidaka, H. (2018) Timing and duration of regional metamorphism in the Kagasawa and Unazuki areas, Hida metamorphic complex, southwest Japan. *Chemical Geology*, **484**: 148–167.

Huang, B.H., 1991. The Permian System of northern Northeast China. In Ishii, K., Liu, X.Y., Ichikawa, K., and Huang, B.H. (Eds.) Pre-Jurassic geology of Inner Mongolia, China, pp. 149–157, Matsuya Insatsu. Osaka.

Ishiwatari, A. and Tsujimori, T. (2003) Paleozoic ophiolites and blueschists in Japan and Russian Primorye in the tectonic framework of East Asia: a synthesis. *Island Arc*, **12**: 190–206.

Isozaki, Y., Aoki, K., Nakama, T. and Yanai, S. (2010) New insight into a subduction-related orogen: Reappraisal on geotectonic framework and evolution of the Japanese Islands. *Gondwana Research* **18**: 82–105.

Isozaki, Y., Aoki, K., Sakata, S. and Hirata, T. (2014) The eastern extension of Paleozoic South China in NE Japan evidenced by detrital zircon U-Pb ages. *GFF*, **136**: 116–119.

Isozaki, Y., Ehiro, M., Nakahata, H., Aoki, K., Sakata, S. and Hirata, T. (2015) Cambrian plutonism in Northeast Japan and its significance for the earliest arc-trench system of proto-Japan: new U-Pb zircon ages of the oldest granitoids in the Kitakami and Ou Mountains. *Journal of Asian Earth Sciences*, **108**:136–149.

Isozaki, Y., Nakahata, H., Zakharov,. Y., Popov, A., Sakata, S. and Hirata, T. (2017) Greater South China extended to

the Khanka block: detrital zircon geochronology of the middle-upper Paleozoic sandstones of the Sergeevka belt, Far East Russia. *Journal of Asian Earth Sciences*, **145**: 565–575.

Isozaki, Y. (2019) A visage of Early Paleozoic Japan; geotectonic and paleobiogeographical significances of Greater South China. *Island Arc*, **28**: e12296.

Iwano, H., Orihashi, Y., Hirata, T., Ogasawara, M., Danhara, T., Horie, K., Hasebe, N., Sueoka, S., Tamura, A., Hayasaka, Y., Katsube, A., Ito, H., Tani, K., Kimura, J., Chang, Q., Kouchi, Y., Haruta, Y. and Yamamoto, K. (2013) An inter-laboratory evaluation of OD-3 zircon for use as a secondary U–Pb dating standard. *Island Arc*, **22**: 382–394.

Izosov, L.A. and Konovalov, Y.I. (2005) The western Sikhote-Alin′ continent-marginal volcanic belt and its tectonic position in the western Pacific continent-ocean transition zone Dal′nauka, Vladivostok, 315 pp. (in Russian).

Jahn, B.M. (2000) Important crustal growth in the Phanerozoic: isotope evidence of granitoids from east-central Asia. *Proceedings of Indian Academy of Science (Earth Planetary Sciences)*, **109**: 5–20.

Kaneoka, I, Matsuda, J., Lelikov, E.P. and S′edin, V.T. (1996) Isotope geochemistry of igneous rocks in the Japan Sea. In Isezaki, N., Bersenev, I.I., Tamaki, K., Karp, B.Y., Lelikov, E.P. (Eds.) Geology and geophysics of the Japan Sea, pp. 369–383, Terrapub, Tokyo. Kano, T. (1990) Granitic rocks in the Hida belt, central Japan. *Mining Geology* **40**: 397–413 (in Japanese with English abstract).

Kemkin, I.V. (2012) Tectono-stratigraphy as a reflection of accretion tectonics processes (on an example of the Nadankhada-Bikin Terrane of the Sikhote-Alin Jurassic accretionary prism, Russia Far East). In Elitok, O. (Ed.) Stratigraphic analysis of layered deposits, InTech, Vladivostok, pp. 279–298.

Khanchuk, A.I., Ratkin, V.V. and Ryazantoseva, M.D. (1996) Geology and mineral deposits of Prymorsky Krai. Dal′nauk, Vladivostok, 56 pp.

Khanchuk, A.I., Kemkin, I.V. and Kruk, N.N. (2016) The Sikhote-Alin orogenic belt, Russian South East: terranes and the formation of continental lithosphere based on geological and isotopic data. *Journal of Asian Earth Sciences*, **120**: 117–138.

Kharchenko, T.A. and Valitov, M.G. (2018) Petrophysical characteristics of the intrusive complexes of different age of the Gamow peninsula (southwestern Primorye). *Russian Journal of Pacific Geology*, **12**: 558–567.

Kojima, S., Kemkin, I.V., Kametaka, M. and Ando, A. (2000) A correlation of accretionary complexes of southern Sikhote Alin of Russia and the Inner zone of southwest Japan. *Geoscience Journal*, **4**: 175–185.

Kotlyar, G., Belyansky, G.C., Burago, V.I., Nikitina, A.P., Zakahrov, Y.D. and Zhuravlev, A.V. (2006) South Primorye, Far East Russia-A key region for global Permian correlation. *Journal of Asian Earth Sciences*, **26**: 28–293.

Kruk, N.N., Golozubov, V.V., Kasatkin, S.A., Rudnev, S.N., Vrzhosek, A.A., Kuibida, M.L. and Vovna, G.M. (2015) Granitoids of the Gamov intrusion (southern Primorye), its peculiarities and indicative and geodynamic role. *Rus-*

sian Geology and Geophysics, **56**: 1685–1700.

Kruk, N.N., Golozubov, V.V., Bayanova, T. B. and Kasatkin, S. A. (2016) Composition, age, and tectonic position of granitoids of the Shmakovka Complex. *Russian Journal of Pacific Geology*, **10**: 132–140.

Kunugiza, K., Shimizu, M. and Otoh, S. (2010) U-Th-Pb chronological constraints on the geotectonic history of central Japan from the Hida metamorphism through the opening of Japan Sea to the present. *Journal of Geological Society of Japan*, **116**: 83–101 (in Japanese with English abstract)

Lelikov, E.P. and Malyarenko, A.N. (1994) Granitoid magmatism of the Pacific marginal seas. Dalʹnauk, Vladivostok, 268 pp. (in Russian)

Lelikov, E.P., Terekhov, E.P. and Yuasa, M. (1996) Pre-Cenozoic stratigraphy of the Japan Sea. In Isezaki, N., Bersenev, I.I., Tamaki, K., Karp, B.Y., and Lelikov, E.P. (Eds.) Geology and geophysics of the Japan Sea, pp.201–222, Terrapub, Tokyo.

Lelikov, E.P. and Pugachev, A.A. (2016) Granitoid magmatism of Japan and Okhotsk Sea. *Petrology*, **24**: 196–213.

Ma, X.H., Zhu, W.P., Zhou, A.H. and Qiao, A.L. (2016) Transformation from Paleo-Asia Ocean closure to Paleo-Pacific subduction: new constraints from granitoids in the eastern Jilin-Heilongjian belt, NE Japan. *Journal of Asian Earth Sciences*, **144**: 261–286.

Maksimov, S.O. and Sakhno, V.G. (2018) Geological and isotope-geochemical criteria for the existence of the ancient continental crust in basement complexes of Primorye. *Doklady Earth Sciences*, **478**: 36–42.

Malinovsky, A.I. and Golozubov, V.V., 2021. Lower Silurian terrigenous rocks of the Laoeling–Grodekovo Terrane, Southern Primorye: composition and formation settings. *Russian Journal of Pacific Geology*, **15**: 1–19.

Melʹnikov, N.G. and Izosov, L.A. (1984). Structure-formation zoning of Primorye. *Tikhookeanskaya Geologiya*, **1**: 53–61 (in Russian).

Nevolin, P.L., Utkin, V.P., Mitrokhin, A.N. and Kutub-Zade, T.K. (2012) Geologic structure of western Primorye: structuring dynamics. *Russian Journal of Pacific Geology*, **6**: 275–293.

Noda, M., 1958. Stratigraphical and palaeontological studodes of the Toman Formation in the Kaishantun and Kamisanbo districts. *Reports Earth Sciences*, *Dept. General Education*, *Kyushu Univ.*, **3**: 1–22.

Oh, C.W. (2006) A new concept of on tectonic correlation between Korea, China and Japan: histories from the late Proterozoic to Cretaceous. *Gondwana Research*, **9**: 47–61.

Otofuji, Y. and Matsuda, T. (1987) Amount of clock-wise rotation of Southwest Japan – fan shaped opening of the southwestern part of the Japan Sea. *Earth and Planetary Science Letters*, **85**: 289–301.

Ovchinnikov, R.O., Sorokin, A.A., Xu, W.L., Yang, H., Kovach, V.P., Kotov, A.B. and Plotkina, Y.V. (2019) Provenance and tectonic implications of Cambrian sedimentary rocks in the Bureya massif, Central Asian orogenic belt, Russia. *Journal of Asian Earth Sciences*, **172**: 393–408.

Paces, J.B. and Miller, J.D. (1993) Precise U-Pb age of Duluth Complex and related mafic intrusions, northern Minnesota: geochronological insights to physical, petrogenetic, paleomagnetic, and tectonomagmatic processes associated with the 1.1 Ga midcontinent rift system. *Journal of Geophysical Research*, **98**: 13997–14013.

Paek, R.J., Kan, H.G., Jon, G.P., Kim, Y.M. and Kim, Y.H. (Eds.), 1993. Geology of Korea. Foreign Language Book Publ. House, Pyongyang, 619 pp.

Sakashima, T., Terada, K., Takeshita, T. and Sano, Y. (2003) Large-scale displacement along the Median Tectonic Line, Japan: evidence from SHRIMP zircon U-Pb dating of granites and gneisses from the South Kitakami and Paleo-Ryoke belts in SW Japan. Journal of Asian Earth Sciences, **21**: 1019–1039.

Sʹedin, V.T., Terekhov, E.P., Gavrilov, A.A., Valitov, M.G. and Kharchenko, T.A. (2018) Formation sequence of igneous and sedimentary rocks of the islands of the central part of the Peter the Great Bay (the Sea of Japan). *Vestnik of the Far East Branch of the Russian Academy of Sciences*, **1**: 128–141.

Sengör, A.M.C. and Natalʹin, B.A. (1996) Plate tectonics of Asia: fragments of a synthesis. In Yin, A. and Harrison, M. (Eds.) The tectonic evolution of Asia, Rubey Colloquim, Cambridge Univ. Press, pp. 486–640.

Shibata, K., Nozawa, T. and Wanless, R.K. (1970) Rb-Sr geochronology of the Hida metamorphic belt, Japan. *Canadian Journal of Earth Science*, **7**: 1383–1401.

Soma, T., Kunugiza, K. and Terabayashi, M. (1990) Hida metamorphic belt. *Fieldtrip Guidebook*, *97th Annual Meeting*, *Geological Society of Japan*: pp. 25–58. (in Japanese)

State Geological Map of the Russian Federation on a scale 1: 200,000, Khanka series, sheets K-52-XII (Vladivostok) and K-52-XVIII (Zarubino) (VSEGEI, St. Petersburg, (2004) (in Russian).

Stacey, J.S. and Krammer, J.D. (1975) Approximation of terrestrial lead isotope evolution by a two-stage model. *Earth and Planetary Science Letters*, **26**: 207–221.

Tagiri, M., Dunkley, D.J., Adachi, T., Hiroi, Y., and Fanning, C.M. (2011) SHRIMP dating of magmatism in the Hitachi metamorphic terrane, Abukuma belt, Japan: evidence for a Cambrian volcanic arc. *Island Arc* **20**: 259–279.

Takahashi, M. (1983) Space-time distribution of late Mesozoic to early Cenozoic magmatism in East Asia and its tectonic implications. In Hashimoto, M. and Uyeda, S. (Eds.) Accretion tectonics in the circum-Pacific regions, pp. 69–88, Terrapub, Tokyo.

Takahashi, Y., Cho, D.L. and Kee, W.S. (2010) Timing of mylonitization in the Funatsu Shear Zone within Hida Belt of southwest Japan: Implications for correlation with the shear zones around the Ogcheon Belt in the Korean Peninsula. *Gondwana Research* **17**: 102–115.

Takahashi, Y., Cho, D.L., Mao, J.R., Zhao, X.L. and Yi, KW. (2018) SHRIMP U-Pb zircon ages of the Hida metamorohic and plutonic rocks in Japan: implications for late Paleozoic to Mesozoic tectonics around the Korean peninsula. *Island Arc*, **27**: e12220.

Takehara, M. and Horie, K. (2019) U-Pb zircon chronology of the Hida gneiss and granites in the Kamioka area, Hida belt. *Island Arc*, **28**: e12303.

Tamaki, K.(1988)Geological structure of the Japan Sea and

its tectonic implications. *Bulletin of Geological Survey of Japan*, **39**: 269–365.

Tazawa, J. (1991) Middle Permian brachiopod biogeography of Japan and adjacent regions in East Asia. In Ishii, K., Liu, X., Ichikawa, K. and Huang, B.H. (Eds.) Pre-Jurassic Geology of Inner Mongolia, China, pp. 213–230, Matsuya-Insatsu, Osaka.

Tsutsumi, Y., Yokoyama, K., Kasatkin, S.A. and Golozubov, V.V., 2014. Zircon U-Pb age of granitoids in the Maizuru Belt, southwest Japan and the southernmost Khanka Massif, Far East Russia. *Journal of Mineralogical Petrological Sciences*, 1**09**: 97–102.

Tsutsumi, Y., Yokoyama, K., Kasatkin, S.A. and Golozubov, V. (2016) Ages of igneous rocks in the southern part of Primorye, Far East Russia. *Bulletin National Museum of Nature and Science, Tokyo*, **51**: 71–78.

Tsutsumi, Y., Isozaki, Y. and Terabayashi, M. (2017) The most continent-sided occurrence of the Phanerozoic subduction-related orogens in SW Japan: Zircon U-Pb dating of the Mizoguchi gneiss on the western foothill of Mt. Daisen volcano in Tottori. *Journal of Asian Earth Sciences*, **145**: 530–541.

Tunheng, A. and Hirata, T. (2004). Development of signal smoothing device for precise elemental analysis using laser ablation-ICP-mass spectrometry. *Journal of Analytical Atomic Spectrometry*, **7**: 932–934.

Ueno, N., Kaneoka, I. and Ozima, M. (1974) Isotope ages and strontium ratios of submarine rocks in the Japan Sea. *Geochemical Journal*, **8**: 157–164.

Vermeesch, P. (2018) IsoplotR: a free and open toolbox for geochronology. *Geoscience Frontiers*, **9**: 1479–1493.

Wang, K.L., Prikhodko, V., O'Reilly, S.O., Griffin, W.L., Pearson, N.J., Kovach, V., Iizuka, Y. and Chien, Y.H. (2015): Ancient mantle lithosphere beneath the Khanka massif in the Russian Far east: in situ Re-Os evidence. *Terra Nova*, **27**: 277–284.

Wilde, S.A. (2015) Final amalgamation of the Central Asian orogenic belt in NE China: Paleo-Asian Ocean closure versus Paleo-Pacific plate subduction—A review of the evidence. *Tectonophysics*, **662**: 345–362.

Williams, I. S. (1998) U–Th–Pb geochronology by ion microprobe. In: McKibben, M. A., Shanks, W.C.P. and Ridley, W.I. (Eds.), Applications of Microanalytical Techniques to Understanding Mineralizing Processes. *Reviews in Economic Geology*, **7**, Society of Economic Geologists, Littleton, CO. USA, pp. 1–35.

Wu, F.Y., Sun, D.Y., Ge, W.C., Zhang, Y.B., Grant, M.L., Wilde, S.A. and Jahn, B.M. (2011) Geochronology of the Phanerozoic granitoids in northeastern China. *Journal of Asian Earth Sciences*, **41**: 1–30.

Xiao, W.J., Windley, B.F., Hao, J. and Zhai, M.C. (2003) Accretion leading to collision and the Permian Solonker suture, Inner Mongolia, China: termination of the Central Asian orogenic belt. *Tectonics*, **22**: 1069.

Yang, H., Ge, W.C,, Zhao, G.C., Yu, J.J. and Zhang, Y.L. (2015) Early Permian-Late Triassic granitic magmatism in the Jiamusi-Khanka massif, eastern segment of the Central Asian orogenic belt and its implications. *Gondwana Research*, **27**: 1509–1533.

Yang, H., Ge, W.C., Bi, J.H., Wang, Z.H., Tian, D.X., Dong, Y. and Chen, H.J. (2018) The Neoproterozoic-early Paleozoic evolution of the Jiamusi Block, NE China and its east Gondwana connection: Geochemical and zircon U-Pb-Hf isotopic constraints from the Mashan Complex. *Gondwana Research*, **54**: 102–121.

Yin, A. and Nie, S. (1993) An indentation model for the North and South China collision and development of the Tanlu and Honan fault systems, eastern Asia. *Tectonics*, **12**: 801–813.

Yokoyama, K. (2012) LA–ICP–MS and SHRIMP ages of zircons in chevkinite and monazite tuffs from the Boso Peninsula, Central Japan. *Bulletin National Museum of Nature and Science Tokyo*, Series C, **38**: 15–32.

Yokoyama, K., Shigeoka, M., Otomo, Y., Tokuno, K. and Tsutsumi, Y. (2016) Uraninite and thorite ages of around 400 granitoids in the Japanese Islands. *Bulletin National Museum of Nature and Science Tokyo*, Series C, **51**: 1–24.

Zhai, M.G., Zhang, Y.B., Zhang, X.H., Wu, F.Y., Peng, P., Li, Q.L., Hou, Q.L., Li, T.S. and Zhao, L. (2016) Renewed profile of the Mesozoic magmatism in Korean Peninsula: Regional correlation and broader implication for cratonic destruction in the North China Craton. *Science China Earth Sciences*, **59**: 2355–2388.

Zakharov, Y.D., Panchenko, I.V. and Khanchuk, A.I. (1992) A field guide to the Late Paleozoic and Early Mesozoic circum-Pacific bio- and geological events. FEGI FEB RAS, Vladivostok, pp.88.

Zhao, X.L., Mao, J.R., Ye, H.M., Liu, K. and Takahashi, Y. (2013) New SHRIMP U-Pb zircon ages ofgranitic rocks in the Hida belt, Japan: implications for tectonic correlation with Jiamusi massif. *Island Arc*, **22**: 508–521.

Zhou, J.B., Wilde, S.A., Zhao, G.C., Zhang, X.Z., Zheng, C.H., Wang, H. and Zeng, W.S. (2010) Pan-African metamorphic and magmatic rocks of the Khanka massif, NE China: further evidence regarding their affinity. *Geological Magazine*, **147**: 737–749.

Zonenshain, L.P., Kuzmin, M.I., and Natapov, L.M. (1990) Geology of the USSR: plate-tectonic synthesis. *American Geophysical Union Geodynamic Series* **21**, 242 pp.